ADVANCED FUNCTIONAL MATERIALS

DOI: 10.1002/adfm.200800099

Band-Edge Engineered Hybrid Structures for Dye-Sensitized Solar Cells Based on SnO_2 Nanowires**

By *Suresh Gubbala, Vidhya Chakrapani, Vivekanand Kumar,* and *Mahendra K. Sunkara**

In this report, we show for the first time that SnO_2 nanowire based dye sensitized solar cells exhibit an open circuit voltage of 560 mV, which is 200 mV higher than that using SnO_2 nanoparticle based cells. This is attributed to the more negative flat band potential of nanowires compared to the nanoparticles as determined by open circuit photo voltage measurements made at high light intensities. The nanowires were employed in hybrid structures consisting of highly interconnected SnO_2 nanowire matrix coated with TiO_2 nanoparticles, which showed an open circuit voltage of 720 mV and an efficiency of 4.1% compared to 2.1% obtained with pure SnO_2 nanowire matrix. The electron transport time constants for SnO_2 nanowire matrix were an order of magnitude lower and the recombination time constants are about 100 times higher than that of TiO_2 nanoparticles. The higher efficiency observed for DSSCs based on hybrid structure is attributed to the band edge positions of SnO_2 relative to that of TiO_2 and faster electron transport in SnO_2 nanowires.

1. Introduction

Over the past decade, TiO_2 nanoparticle films have been used widely for dye sensitized solar cells (DSSC).[1,2] The electron injection rates from the excited dye into the TiO_2 nanoparticles are ultra-fast, on the order of femto seconds, but the electron recombination rates are high due to low electron mobility and transport properties.[3] Thus, there has been an interest in search for alternate materials and assemblies. ZnO and Nb_2O_5 are possible candidates, since they have a more negative conduction band edge than TiO_2, but suffer from chemical instability and poor dye adsorption properties.[4,5] Tin oxide (SnO_2) on the other hand is a promising wide band gap oxide material because of its higher electronic mobility and large band gap (3.8 eV). Mobility reported in both single crystal SnO_2 ($\mu_e \sim 250\,cm^2\,V^{-1}\,s^{-1}$)[6] as well as nanostructures ($\mu_e \sim 125\,cm^2\,V^{-1}\,s^{-1}$)[7] are orders of magnitude higher than in both single crystal TiO_2 ($\mu_e < 1\,cm^2\,V^{-1}\,s^{-1}$)[3] and ZnO ($\mu_e \sim 1$–$5\,cm^2\,V^{-1}\,s^{-1}$).[8] Furthermore, SnO_2 has a low sensitivity to UV degradation due to its larger band gap and hence has better long term stability.[9] In spite of these advantages the open circuit voltage, V_{oc}, of SnO_2 nanoparticle based DSSCs has been limited to less than 400 mV,[10–14] making them less attractive. Various attempts to improve the efficiencies of SnO_2 nanoparticle based cells such as electrode surface and electrolyte modification to improve the dye attachment,[14,15] mixing with nanoparticles of other materials,[12,16–18] and coating with thin layer of other oxide materials to form core-shell structures have resulted in moderate improvements in efficiency.[9,19–22]

The main drawback for any nanoparticle (NP) based cells is poor interconnectivity between particles that results in high recombination losses and low fill factor.[23] Nanowires (NW) on the other hand are promising for DSSC because they can provide faster electron transport for the injected electrons to the back contact. The use of nanowire arrays was first proposed for photoelectrochemical generation of hydrogen from water,[24] followed by reports on their use in DSSC.[23,25–27] Although, the majority of the reports on DSSC used vertically aligned nanowires on conducting substrates for fast electron transport, the morphology and orientation of nanowires is shown to play an important role in enhancing the dye loading and light absorption specifically indicating that the photon absorption and fill factor are better with "flower-like" structures compared to vertical arrays.[28] In the current work, we used nanowire powder containing highly branched and interconnected SnO_2 nanowires to fabricate a dense matrix. This method will allow for large scale manufacturing of solar cells on a roll to roll basis on flexible substrates.

Most importantly, the use of NWs allows the implementation of hybrid structures designed based on band-edge engineering. In this work, hybrid electrodes were fabricated by coating SnO_2 nanowire matrix with TiO_2 nanoparticles. See Figure 1 for the energy band diagram of SnO_2, TiO_2, and N719 dye at pH = 1 with respect to the electrochemical scale. The conduction band edge of SnO_2 is 0.4 V more positive than that of TiO_2. Thus the electrons injected into TiO_2 from the excited

[*] Prof. M. K. Sunkara, S. Gubbala, Dr. V. Chakrapani, V. Kumar
Department of Chemical Engineering, University of Louisville
Louisville, 40292 (USA)
E-mail: mahendra@louisville.edu

[**] The authors gratefully acknowledge support from the U.S. Department of Energy for Institute of Advanced Materials at the University of Louisville (DE-FG02-05ER64071) and DoE-EPSCoR program (DE-FG02-07ER46375). Supporting Information is available online from Wiley InterScience or from the authors.

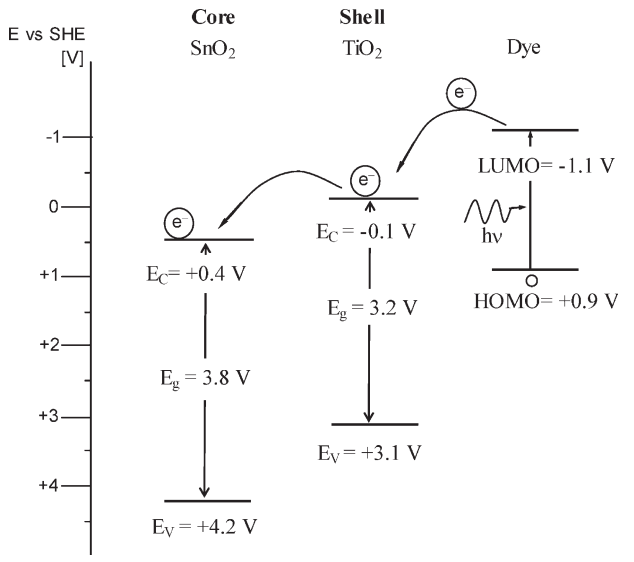

Figure 1. Energy band diagram of SnO_2, TiO_2 and N719 dye with respect to the electrochemical scale at pH = 1.

dye will be efficiently injected into SnO_2. The excellent transport properties of interconnected nanowires should allow fast transport of electrons to the back contact, thus lowering the recombination rate. Thus in principle one can tailor the properties of hybrid DSSC to maximize the efficiency by choosing different semiconductors with appropriate band lineup and electronic properties.

2. Results and Discussion

The SEM images in Figure 2 show morphologies of the as-synthesized nanowires. The sizes of SnO_2 nanowires ranged from 20 nm to 200 nm in diameter and lengths up to a few tens of micrometers depending on the growth conditions. In this method, the growth of nanowires follows that of a self catalytic vapor-liquid-solid (VLS) mechanism.[29] The branching and interconnectivity of nanowires is promoted by providing Sn droplets intermittently for secondary nucleation. This is done by fluctuating the temperatures of both the Sn source and the substrate (see Fig. 2b). In the case of excess Sn in the initial stages, oxidation proceeds via spontaneous nucleation of high density of nanowires from large size Sn droplets leading to flower-like morphologies (Fig. 2d).[30,31]

Figure 3 shows the SEM image of hybrid electrodes fabricated using SnO_2 nanowires. The diameters of the SnO_2 nanoparticles coated on the nanowires were found to be in the range of 20–40 nm. It is interesting to note that on the nanowires, the SnO_2 particles aggregates into clusters. On the other hand, the TiO_2 particles form a uniform coating along the length of nanowires. The diameters of TiO_2 nanoparticles ranged from 5 to10 nm. The XRD spectrum of the TiO_2 coated nanowires confirmed that they were highly crystalline phases of SnO_2 nanowires and rutile phase TiO_2 nanoparticles. Figure 3c shows the morphology of ALD coating of TiO_2 onto SnO_2 NW. Figure 3d shows the SEM of the 20–30 nm sized, commercially obtained tin oxide nanoparticles.

Figure 4 shows the current–voltage characteristics of DSSCs made using four different types of SnO_2 materials. The various cell parameters obtained from the data shown in Figure 4a are summarized in Table 1. The electrodes made using nanowires irrespective of their size and morphology consistently showed higher open circuit voltage (V_{oc} = 520–560 mV) and fill factor (FF = 0.5) than the nanoparticles electrodes (V_{oc} = 350 mV and FF = 0.36). However, the higher current density of the nanoparticle based DSSC (I_{sc} = 11 mA cm^{-2}) can be attributed to their higher surface area (Roughness factor ~900) compared to the nanowire (5.7 mA cm^{-2}) based electrodes (Roughness factor ~100–200) fabricated here. The roughness factors were estimated using both the weights of materials used within the films of similar thicknesses (25–30 μm) and the specific surface areas determined using BET isotherms for sintered nanowire and nanoparticle samples. In the case of NWs, the surface roughness factors were different between samples produced in separate synthesis experiments due to differences with the diameter distribution and the interconnectivity in the resulting nanowire powders. In terms of different nanowire samples, the current density was highly dependent on the morphology of the wires. Typically, current densities ranged from 1 mA cm^{-2} for individual nanowires to 6 mA cm^{-2} for the thin, highly branched, nanowire based electrodes. Higher efficiencies were observed for electrodes made using branched and highly interconnected nanowire samples (2.1%) compared to the electrodes made using powder containing mainly individual NWs (0.58%). The efficiency values reported above were estimated using the transmitted light intensity through the FTO substrate (~70 mW cm^{-2}). The overall efficiency values for these cells without considering 30% transmission loss through the FTO substrate are approximately 1.5% and 0.4%, respectively. It should however be noted that some studies in literature have used conducting glass substrates with anti-reflective coatings that can give over 95% transmission.[32] In this case, the efficiency values reported while correcting for the transmission loss for the specific FTO substrates used would be most appropriate.

As shown in Figure 4, the V_{oc} of all nanowire electrodes was observed to be greater than 520 mV (typically closer to 560 mV) irrespective of the size and morphology of NWs. These values are about 200 mV higher than the typical V_{oc} values for nanoparticle electrodes reported here and elsewhere. Figure 5 shows the changes in the open circuit potential of SnO_2 nanowire and nanoparticle DSSC's with increasing light intensity. The V_{oc}, which is the difference between the Fermi level in the semiconductor and the redox potentials of I^-/I_3^-, of all the electrodes increased with increased light intensity and saturated at high light intensities. The measured V_{oc} values under high light intensities can give a rough estimate of the Fermi level position assuming that it is not limited by the charge injection from the dye. In the measured intensity range, the maximum value of V_{oc} of nanowire electrode is 250 mV

ADVANCED FUNCTIONAL MATERIALS

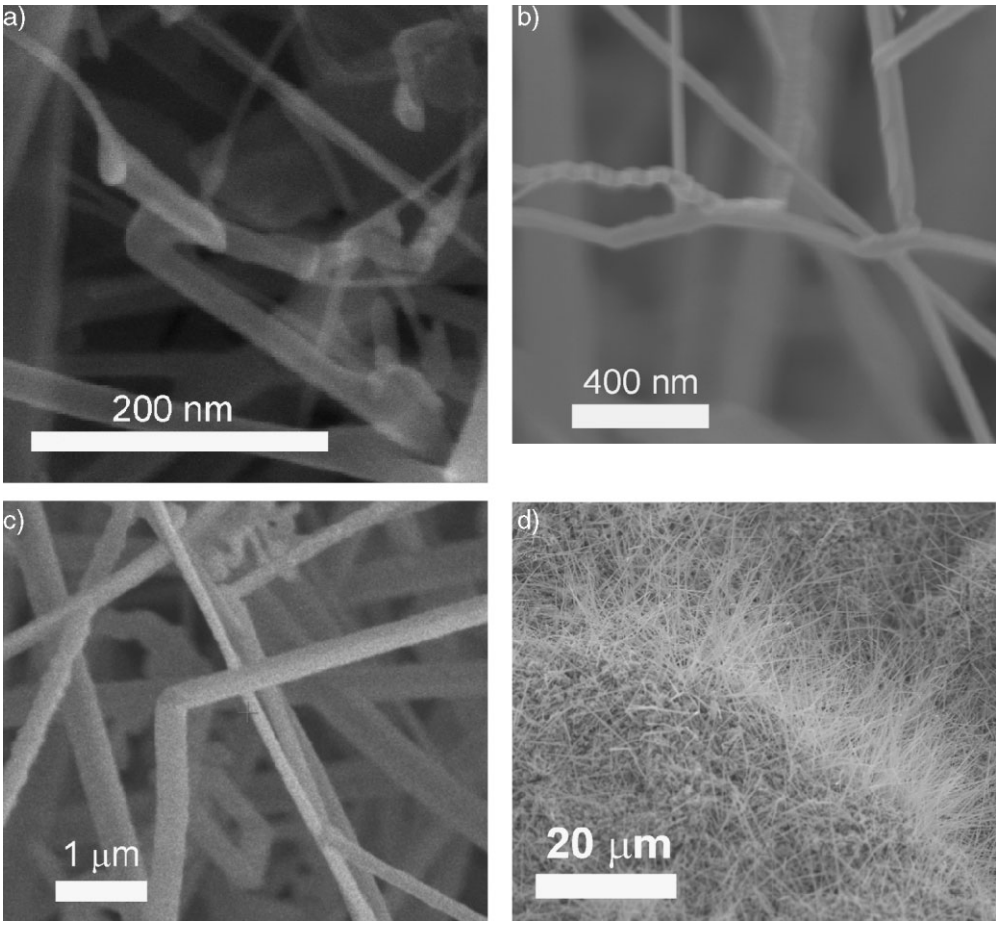

Figure 2. Representative SEM images of the as-synthesized a) straight tin oxide nanowires, b) branched tin oxide nanowires c) large diameter, low aspect ratio SnO_2 nanowires, and d) tin oxide nanowires growing out of one single droplet of tin during initial growth. Longer experiments lead to the complete conversion of tin droplets into nanowires.

higher than the nanoparticle electrode. Assuming the potential of I^-/I_3^- at +0.4 V versus SHE, the flat band potentials estimated for SnO_2 nanoparticle, and nanowire electrodes were +0.1 V versus SHE, and −0.16 V versus SHE, respectively. The Mott–Schottky analysis also showed similar difference between the flat band potentials for nanoparticle and nanowire electrodes. However, the data exhibited large frequency dependence and thus is not considered further for estimating the absolute position of the flat band potential. Nevertheless, one must still explain the origin for the observed difference between Fermi level positions of nanowire and nanoparticle electrodes from the observed, open circuit potentials. Since nanowires typically have only one or two types of facets, the surface of all nanowires could represent that of a single crystal surface. Such faceted structures have been observed for other nanowire systems also. For example, in the case of GaN, such faceting was clearly observed after homoepitaxial growth on thin (<30 nm) nanowires to form belts and thicker wires depending on the growth direction of the starting nanowire.[33] In fact, the measured value of the flat band potential for SnO_2 nanowire electrode determined using the open circuit potential at high light intensities is close to the flat band potential value (approximately −0.1 vs. SHE at pH = 7) for single crystal electrode determined using Mott–Schottky analysis.[34] Nanoparticles on the other hand have mixed facets and a large number of edge sites leading to a high degree of surface polycrystallinity. Such shifts in the flat band potential with crystallographic orientation have also been noted before in other materials.[35,36] Further in-depth work is underway using ultraviolet photoelectron spectroscopy (UPS), Kelvin probe along with Mott–Schottky analysis to determine the absolute positions of Fermi level and conduction band edge in both nanoparticle and nanowire electrodes.

The data in Figure 4a suggests that the SnO_2 nanoparticle coated SnO_2 nanowire DSSC's showed a very little increase ($I_{sc} = 6.3\,mA\,cm^{-2}$) in the short circuit current compared to SnO_2 nanowire electrodes ($I_{sc} = 5.7\,mA\,cm^{-2}$) while the value of their open circuit potentials (484 mV) were between those of SnO_2 nanoparticle (356 mV) and SnO_2 nanowire electrodes (522 mV). The TiO_2-SnO_2 hybrid structures showed the highest efficiencies (4.1%), with a high short circuit current ($8.56\,mA\,cm^{-2}$) and open circuit voltage (686 mV). The current

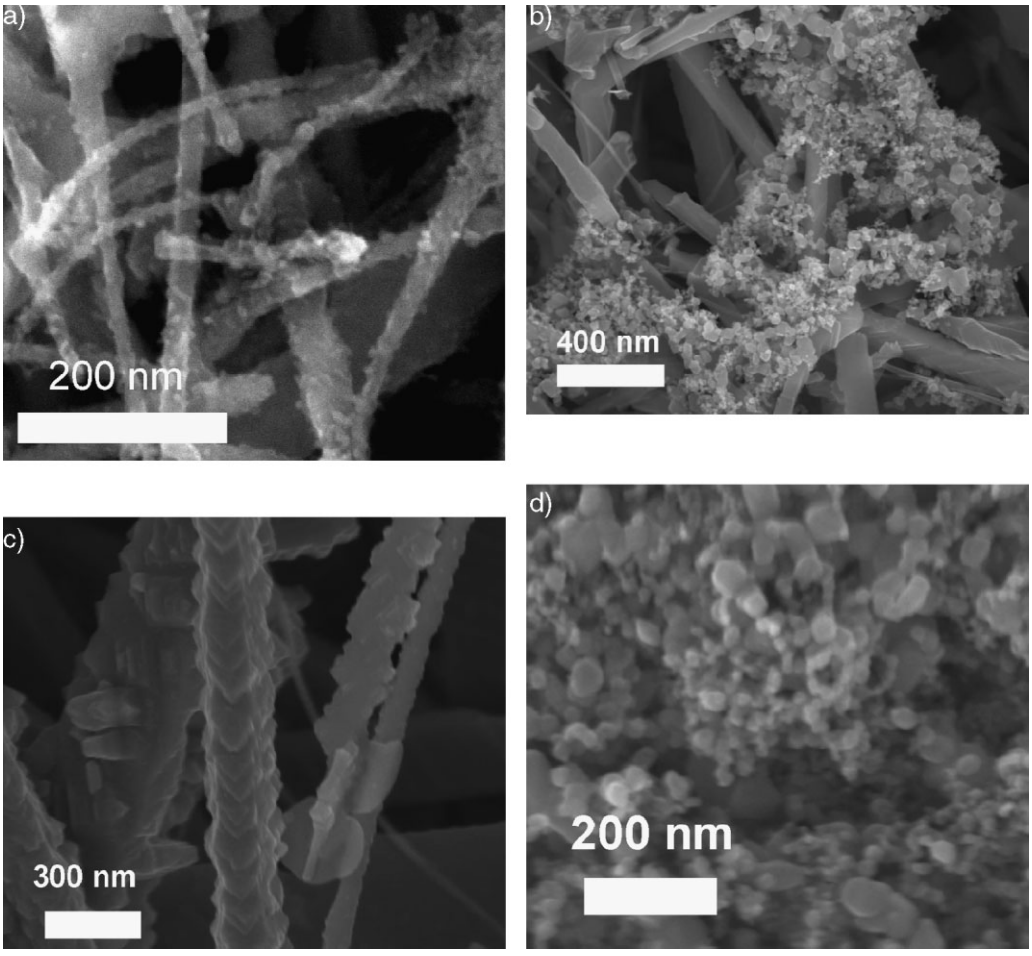

Figure 3. Representative SEM images of the fabricated electrodes a) SnO_2 nanowires coated with TiO_2 nanoparticles, b) SnO_2 nanowires coated with SnO_2 nanoparticles, c) SnO_2 nanowires coated with a layer of TiO_2 by atomic layer deposition, and d) SnO_2 nanoparticles.

densities of the TiO_2-SnO_2 hybrid electrodes depended on the morphology of SnO_2 nanowires used and typical values for samples made in this work ranged from 3 to 9 mA cm^{-2}. At high light intensity, the maximum voltage shown by the hybrid electrode was ~750 mV, corresponding to −0.35 V versus SHE. If one were to calculate the efficiency without correcting for the transmission loss from FTO substrate, the efficiency value is about 2.9%. The corresponding IPCE curves are shown in Figure 4b. The higher IPCE values of the nanoparticle electrode compared to nanowire electrode is due to their higher surface area and higher dye loading. Also, both the absorption spectra and the IPCE spectra obtained for another set of SnO_2 nanoparticle and nanowire electrodes illustrate the same aspect (shown in the Supporting Information). Note that these electrodes have different thickness and are prepared using a different batch of nanowires than those used for the data in Figure 4.

In order to understand the differences observed with different electrodes in Figure 4, we conducted photocurrent and photovoltage decay measurements. Figure 6 shows the photocurrent decay measurements for different electrodes. The current responses were fitted using first order decay kinetics and the time constants were obtained accordingly and summarized in Table 2. The transport time constants of various nanowire samples were varied depending upon how well they are interconnected and branched. These values ranged from 4.5 ms for high aspect ratio branched nanowires to 30 ms for low-aspect ratio loosely connected wires. Also, the electron transport in the nanowire electrode is generally found to be faster than the nanoparticle electrode ($\tau = 17$ ms). Earlier, much dramatic improvement in the electron transport was reported for ZnO NW array ($\tau = 30$ μs) compared to its counterpart NP cells ($\tau = 10$ ms).[37] Fast current decay in nanowire based electrodes in these cell indicates a higher diffusion constant (D_n) for electron transport through them (since the film thicknesses are almost the same). Since the electron diffusion length (L_n) in the electrode is directly related the diffusion coefficient and the electron recombination time constant (τ_r) by the relation $L_n = (D_n \tau_r)^{1/2}$, it is clear that the electron diffusion lengths in the nanowire based cells are longer than the nanoparticle based cells. The longer diffusion length of the electrons in these films means that the

ADVANCED FUNCTIONAL MATERIALS

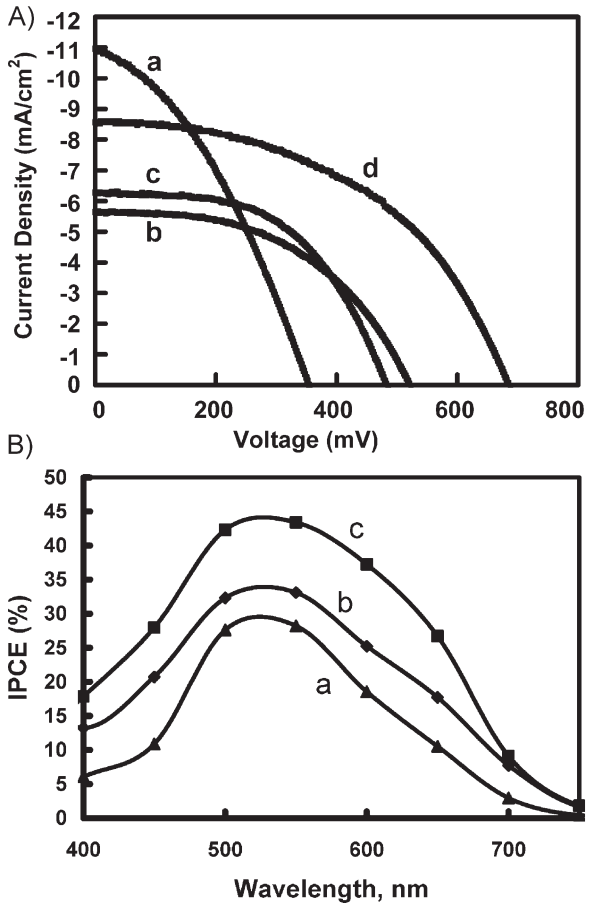

Figure 4. A) *I–V* characteristics of the solar cells made from a) SnO_2 nanoparticles, b) SnO_2 nanowires, c) SnO_2 nanowires coated with SnO_2 nanoparticles, and d) SnO_2 nanowires coated with TiO_2 nanoparticles. B) IPCE spectra of a) SnO_2 nanowires, b) SnO_2-TiO_2 hybrid structure, and c) SnO_2 nanoparticles.

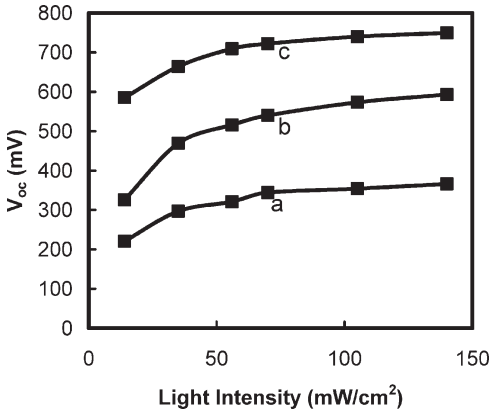

Figure 5. Open circuit potential measurements at different light intensities for (a) SnO_2 nanoparticles, (b) SnO_2 nanowires and (c) SnO_2-TiO_2 hybrid structure.

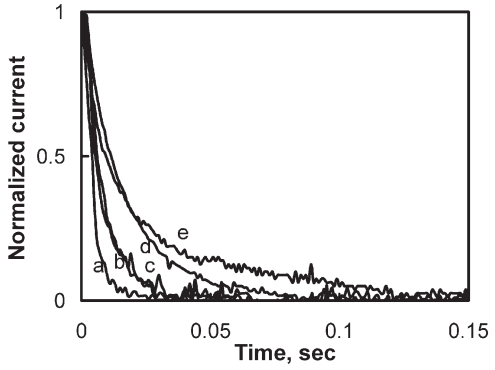

Figure 6. Transient photocurrent decay measurements for solar cells made from a) SnO_2 nanowires, b) SnO_2 nanowires coated with TiO_2 nanoparticles, c) SnO_2 nanowires coated with SnO_2 nanoparticles, d) SnO_2 nanoparticles, and e) TiO_2 nanoparticles.

electrons travel farther in the film before they recombine with the electrolyte solution, thus decreasing the recombination reaction. The time constants for electron transport in hybrid electrodes consisting of SnO_2 nanoparticle coated nanowires (9 ms) and TiO_2 nanoparticle coated nanowires (9 ms) was also observed to be close to the transport constants for the bare SnO_2 nanowire electrodes.

Figure 7 shows the changes in the dark recombination current with applied bias. This current is indicative of the recombination of the electrons with the electrolyte. The onset of recombination current occurs at higher potential for

Table 2. Summary of the transport properties of solar cells made using different materials. The nanowire based DSSCs were made using high aspect ratio, interconnected nanowires.

Transport time constants [ms]	
SnO_2 NP	17
TiO_2 NP	25
SnO_2 NW	4.5
SnO_2 NW coated with TiO_2 NP	9
SnO_2 NW coated with SnO_2 NP	9

Table 1. Summary of performance of the different kinds of cells tested using 100 mW cm^{-2} light intensity (or about 70 mW cm^{-2} transmitted through FTO substrate).

Solar Cell Characteristics		J_{sc} [mA cm^{-2}]	V_{OC} [mV]	Fill Factor	Efficiency [%]
SnO_2 NP		11	356	0.36	2
High aspect ratio,	SnO_2 NW	5.7	522	0.5	2.1
interconnected nanowires	SnO_2 NW coated with SnO_2 NP	6.3	484	0.53	2.3
	SnO_2 NW coated with TiO_2 NP	8.56	686	0.49	4.1
Low aspect ratio,	SnO_2 NW	1.23	560	0.59	0.58
thick nanowires	SnO_2 NW coated with TiO_2 NP	1.39	720	0.61	0.87
	SnO_2 NW coated with ALD TiO_2	2	725	0.62	1.29

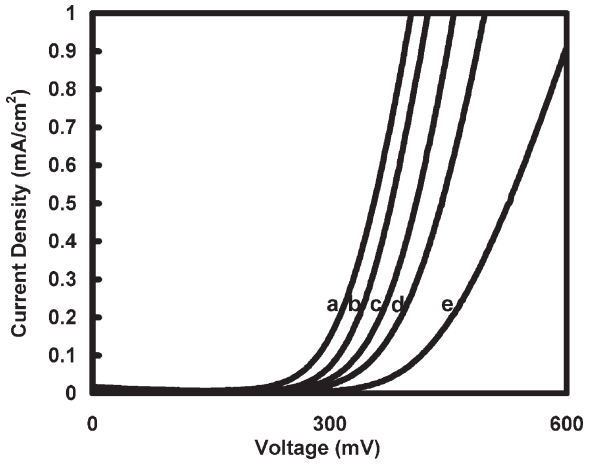

Figure 7. Dark recombination currents for electrodes made with a) SnO_2 nanoparticles, b) SnO_2 nanowires coated with SnO_2 nanoparticles, c) SnO_2 nanowires, d) SnO_2 nanowires coated with TiO_2 nanoparticles, and e) SnO_2 nanowires coated with a layer of TiO_2 by atomic layer deposition.

nanowire electrodes when compared to the nanoparticle electrodes. The charge leakage from the nanoparticles may be mediated by traps whose energy shifts with applied potential. One of the reasons for the observed low fill factor for nanoparticle electrode (see Fig. 4) is probably due to the influence of bias induced acceleration of electron recombination kinetics. This would lower the fill factor. Higher recombination reactions decrease the electron density in the semiconductor phase, which lowers the resulting open circuit voltage.

Figure 8 shows the electron recombination lifetime for different electrodes. The recombination lifetimes were calculated from the open circuit potential decay curves. The values were obtained from the expression

$$\tau_r = -\left(\frac{kT}{e}\right)\left(\frac{dV_{OC}}{dt}\right)^{-1} \quad (1)$$

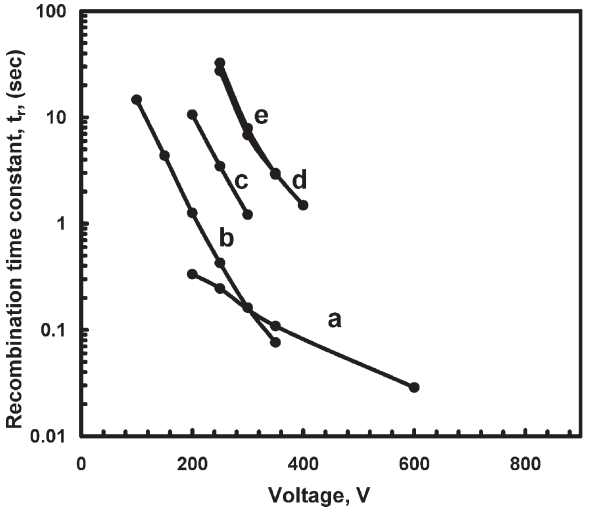

Figure 8. Electron recombination time constants for a) TiO_2 nanoparticles, b) SnO_2 nanoparticles, c) SnO_2 nanowires coated with SnO_2 nanoparticles, d) SnO_2 nanowires, and e) SnO_2 nanowires coated with TiO_2 nanoparticles.

The SnO_2 nanowire DSSC's show about two orders of magnitude slower recombination rate than the SnO_2 nanoparticle and also TiO_2 nanoparticle based DSSC over the entire range of V_{oc} values. Hybrid structures consisting of SnO_2 nanoparticle coated SnO_2 nanowire DSSCs showed a recombination time constant that was between that of the pure SnO_2 nanoparticle and SnO_2 nanowire DSSC's. It was also observed that the recombination time constant for TiO_2 nanoparticle coated SnO_2 nanowire electrodes was very close to that of pure SnO_2 nanowire based DSSCs, which was about two orders of magnitude slower than pure TiO_2 nanoparticles. Faster transport through the nanowires can only partially explain the observed differences with recombination kinetics in the nanoparticle and nanowire electrodes. Further in-depth work is being carried out to understand the differences in the electronic properties of nanoparticles and nanowires.

Even though, the hybrid structures consisting of SnO_2 or TiO_2 nanoparticles on SnO_2 nanowires were not optimized for their best performance, a two fold increase in the efficiencies were clearly observed when compared to the pure SnO_2 NW DSSC and TiO_2 nanoparticle electrodes which were fabricated in a similar fashion (Supporting Information). Although the efficiencies observed for TiO_2 nanoparticle based electrodes are low, such values been reported previously.[23,38,39] For SnO_2 NP-NW cell, the higher surface area of SnO_2 nanoparticles made a small improvement to the J_{sc}. Both SnO_2 NW-NP and SnO_2 NW/TiO_2 systems had a similar transport time constant (9 ms), similar to that of pure SnO_2 NW electrode (see Table 2) which is expected since the transport properties are primarily determined by the underlying matrix material. Hence, the electron transport through TiO_2 can be increased up to 10 times by employing them in hybrid cells involving SnO_2 type semiconducting matrix. The faster electron transport of hybrid cells also decreases the rate of recombination by 2 orders of magnitude. It is interesting to note that both the V_{oc} and the recombination properties of SnO_2 NP-NW cell shows mixed properties of both NP and NW cell. The V_{oc} of the hybrid cell probably depends on the ratio of total surface area of NPs and NWs exposed to the dye. The $TiCl_4$ treatment on the other hand results in almost uniform coverage of TiO_2. In this case, the V_{oc} for SnO_2/TiO_2 is almost same as that of a pure TiO_2 based DSSC. The fast electron transfer from TiO_2 to SnO_2 due to the respective positioning of band edges and subsequent fast transport through SnO_2 is expected to lower the recombination and lead to higher current densities.

ALD coatings of TiO_2 on SnO_2 nanowires also resulted in an improvement in the short circuit current and the open circuit voltage. Figure 7 compares the dark recombination current for

ADVANCED FUNCTIONAL MATERIALS

all the above mentioned electrodes. The recombination current is smaller for the nanowire based cells, compared to the nanoparticle based cells. Further, SnO_2 nanoparticle treated films show recombination current characteristics which are between nanoparticles and nanowires. TiO_2 nanoparticle treated films show a lower recombination current than nanowire films and an even greater suppression of the dark current is seen in TiO_2 ALD coated films. Similar results were shown using semiconducting single walled carbon nanotube (SWNT) matrix coated with TiO_2 based PEC cells in which the band-edges allow for faster electron transfer from TiO_2 to SWNTs.[40]

However, the band-edge engineered hybrid structures are not possible by employing core-shell type particles. In core-shell nanoparticles, the electron transport occurs primarily through the interconnected shell particles as there is high transport resistance between individual core particles. Several authors have reported ZnO/TiO_2 and TiO_2/SnO_2 core shell DSSC's have lower short circuit current and efficiency.[41,42] The CBM of ZnO is higher than that of TiO_2 and thus presents a barrier for electron transport from TiO_2 to ZnO. This results in lower J_{sc}.

The efficiencies reported here with our hybrid assembly of SnO_2 NWs coated with TiO_2 nanoparticles can further be improved by optimizing the NW film thickness, NW size, interconnectivity, NW film density, and TiO_2 NP loading. Most importantly, the paper provides a scheme for designing novel hybrid structures for DSSCs that can lead to very high efficiency cells. For example, controlled alloying with other materials can also be used to tune the band edges with respect the redox couple to maximize the efficiency. These designs could easily be extended to include several new oxide (tungsten oxide and iron oxide) and nitride materials for DSSC that have otherwise been thought to perform poorly.

3. Conclusions

The DSSC made using SnO_2 nanowires show 200 mV higher open circuit voltages compared to those based on nanoparticles. The shift in the open circuit voltages arises due to the differences in the position of bulk Fermi level in the two materials, as illustrated by the open circuit photo voltage measurements at high light intensities. The electron transport through the SnO_2 nanowire matrix is found to be an order of magnitude faster than the nanoparticles. The performance of DSSC made using SnO_2 nanowire powders is dependent on the morphologies of the as-synthesized nanowires, i.e., branched and interconnected nanowires yield the maximum efficiency. The performance of these nanowire electrodes were further improved by employing them in hybrid structures consisting of conducting SnO_2 nanowire matrix coated with TiO_2 nanoparticles. Both the transport and recombination properties of TiO_2 showed significant improvement when employed in hybrid cells. This is because the electron transfer between TiO_2 to SnO_2 occurs fast due to the proper line-up of band edges followed by fast transport through SnO_2 nanowire matrix.

4. Experimental

SnO_2 nanowires were synthesized on quartz substrates by reactive vapor transport method using Sn metal as the tin source in oxygen (5 sccm) and hydrogen (200 sccm). The temperature of the heater was 1100 °C and that of the quartz substrate was 850 °C and the pressure was 700 mTorr. The heater was switched on and off periodically during the synthesis to grow branched and highly interconnected nanowire structures over a total period of 30 minutes. Low aspect ratio, thick nanowires were grown at 1400 °C. The nanowires deposited on the quartz substrate were scraped and dispersed in a mixture of water and Triton-X surfactant. The suspension was sonicated and then centrifuged to obtain a uniform paste. The paste was then mixed with a 1:4 mixture of ethyl cellulose and terpiniol (weight equal to that of nanowires) to facilitate the easy spreading on the FTO glass piece. The electrodes were prepared by depositing the paste on the FTO glass slide using the doctor blade technique, followed by sintering at 575 °C for 1 hour. The thickness of the deposited electrodes was 25–30 μm. Films thicker than these were mechanically unstable. The preparation technique for the nanoparticles electrodes were similar to the nanowire electrode except the paste was made using commercially available SnO_2 and TiO_2 nanoparticles (Alfa Aesar and Aldrich). The surface area of the electrodes was determined by BET measurements (Micromeritics Tristar 3000).

Hybrid structures were prepared by coating the SnO_2 nanowires with SnO_2 or TiO_2 nanoparticles. The coating with SnO_2 nanoparticles was done by immersing the SnO_2 nanowire electrodes in SnO_2 nanoparticles in water (0.2 M) and Triton-X surfactant for 1 h. Two different methods were used to deposit TiO_2 onto the nanowires. In the first method the nanowire electrodes were dipped in a $TiCl_4$ aqueous solution (0.2 M) for 1 h and sintered again at 400 °C for 1 h. In the second method, a thin layer of TiO_2 was deposited using an atomic layer deposition (ALD) system (Cambridge Instruments Savannah 100). ALD was performed at 600 mTorr pressure and a temperature of 300 °C with water and titanium isopropoxide as the precursor materials. The deposition was done for 200 cycles which resulted in a coating thickness of ~10 nm.

The electrodes, with an active cell area of 0.25 cm^2, were immersed in a 0.5 mM L^{-1} Ru-535-bisTBA (also known as N719, Solaronix, Switzerland) sensitizer dye in absolute ethanol for ~18 hours. The excess dye from the electrodes was rinsed with ethanol. Although, the N719 dye may not be ideal for SnO_2, it is primarily used to compare the performance of different electrodes and the concept of hybrid structures studied here. The solar cells were made by assembling these electrodes with a platinum coated FTO counter electrode, and filled with the I^-/I_3^- redox electrolyte (Iodolyte, Solaronix). The cells were sealed with Surlyn sealant (Solaronix). The cells were illuminated from the semiconductor side using a 100 mW cm^{-2} power AM 1.5 filtered Xenon light source (Newport Instruments). The light intensity decreased to ~70 mW cm^{-2} from 100 mW cm^{-2} upon passing through the FTO glass. The efficiency values were, therefore calculated based on 70 mW cm^{-2} light intensity. Transient photocurrent decay measurements done using a 650 nm laser source with a pulse intensity of 15 mW cm^{-2} superimposed on a background illumination intensity of 50 mW cm^{-2}.

The time constant for electron transport, τ_c, was determined by fitting an exponential curve to the photocurrent decay data. This technique has previously been discussed by Boschloo et al. [43]. Open circuit photovoltage decay measurements, as described by Zaban et al. [44], were done to determine the electron recombination time constants, which was determined from Equation 1. All solar cell fabrication and measurements were done in ambient atmosphere. The

electrochemical measurements were performed using an EG&G Princeton Applied Research 273A potentiostat.

Received: January 21, 2008
Revised: May 2, 2008

[1] B. O. Regan, M. Grätzel, *Nature* **1991**, *353*, 737.
[2] M. K. Nazeeruddin, A. Kay, I. Rodicio, R. Humphry-Baker, E. Muller, P. Liska, N. Vlachopoulos, M. Grätzel, *J. Am. Chem. Soc.* **1993**, *115*, 6382.
[3] E. Hendry, M. Koeberg, B. O'Regan, M. Bonn, *Nano Lett.* **2006**, *6*, 755.
[4] M. Grätzel, *Nature* **2001**, *414*, 338.
[5] *Photoelectrochemistry, Photocatalysis and Photoreactors Fundamentals and Developments* (Ed: M. Schiavello), Springer, New York **1985**.
[6] Z. M. Jarzebski, J. P. Marton, *J. Electrochem. Soc.* **1976**, *123*, 299C.
[7] M. S. Arnold, P. Avouris, Z. W. Pan, Z. L. Wang, *J. Phys. Chem. B* **2003**, *107*, 659.
[8] C. H. Seager, S. M. Myers, *J. Appl. Phys.* **2003**, *94*, 2888.
[9] N. G. Park, M. G. Kang, K. S. Ryu, K. M. Kim, S. H. Chang, *J. Photochem. Photobiol. A* **2004**, *161*, 105.
[10] S. Chappel, A. Zaban, *Sol. Energy Mater. Sol. Cells* **2002**, *71*, 141.
[11] K. Sayama, H. Sugihara, H. Arakawa, *Chem. Mater.* **1998**, *10*, 3825.
[12] J. Bandara, K. Tennakone, *J. Colloid Interface Sci.* **2001**, *236*, 375.
[13] Y. Fukai, Y. Kondo, S. Mori, E. Suzuki, *Electrochem. Commun.* **2007**, *9*, 1439.
[14] N. N. Dinh, M. C. Bernard, A. H. L. Goff, T. Stergiopoulos, P. Falaras, *C. R. Chim.* **2006**, *9*, 676.
[15] G. Vilaca, B. Jousseaume, C. Mahieux, C. Belin, H. Cachet, M. C. Bernard, V. Vivier, T. Toupance, *Adv. Mater.* **2006**, *18*, 1073.
[16] K. Tennakone, G. R. R. A. Kumara, I. R. M. Kottegoda, V. P. S. Perera, *Chem. Commun.* **1999**, 15.
[17] G. R. A. Kumara, A. Konno, K. Tennakone, *Chem. Lett.* **2001**, 180.
[18] C. Nasr, P. V. Kamat, S. Hotchandani, *J. Phys. Chem. B* **1998**, *102*, 10047.
[19] A. Keys, M. Grätzel, *Chem. Mater.* **2002**, *14*, 2930.
[20] G. R. R. A. Kumara, K. Tennakone, V. P. S. Perera, A. Konno, S. Kaneko, M. Okuya, *J. Phys. D* **2001**, *34*, 868.
[21] K. Tennakone, J. Bandara, P. K. M. Bandaranayake, G. R. R. A. Kumara, A. Konno, *Jpn. J. Appl. Phys.* Part 2 **2001**, *40*, L732.
[22] M. K. I. Senevirathna, P. K. D. D. P. Pitigala, E. V. A. Premalal, K. Tennakone, G. R. A. Kumara, A. Konno, *Sol. Energy Mater. Sol. Cells* **2007**, *91*, 544.
[23] K. Zhu, N. R. Neale, A. Miedaner, A. J. Frank, *Nano Lett.* **2007**, *7*, 69.
[24] N. Beermann, L. Vayssieres, S. E. Lindquist, A. Hagfeldt, *J. Electrochem. Soc.* **2000**, *147*, 2456.
[25] J. B. Baxter, E. S. Aydil, *Appl. Phys. Lett.* **2005**, *86*, 053114 (1–3).
[26] M. Law, L. E. Greene, J. C. Johnson, R. Saykally, P. Yang, *Nat. Mater.* **2005**, *4*, 455.
[27] G. K. Mor, K. Shankar, M. Paulose, O. K. Varghese, C. A. Grimes, *Nano Lett.* **2006**, *6*, 215.
[28] C. Y. Jiang, X. W. Sun, G. Q. Lo, D. L. Kwong, J. X. Wang, *Appl. Phys. Lett.* **2007**, *90*, 263501 (1–3).
[29] S. Vaddiraju, A. Mohite, A. Chin, M. Meyyappan, G. Sumanasekera, B. W. Alphenaar, M. K. Sunkara, *Nano Lett.* **2005**, *5*, 1625.
[30] R. Rao, H. Chandrasekaran, S. Gubbala, M. K. Sunkara, C. Doraio, S. Jin, A. M. Rao, *J. Electron. Mater.* **2006**, *35*, 941.
[31] S. Sharma, M. K. Sunkara, *J. Am. Chem. Soc.* **2002**, *124*, 12288.
[32] S. Ito, S. M. Zakeeruddin, R. Humphry-Baker, P. Liska, R. Charvet, P. Comte, M. K. Nazeeruddin, P. Péchy, M. Takata, H. Miura, S. Uchida, M. Grätzel, *Adv. Mater.* **2006**, *18*, 1202.
[33] H. Li, A. Chin, M. K. Sunkara, *Adv. Mater.* **2006**, *18*, 216.
[34] J. M. Bolts, M. S. Wrighton, *J. Phys. Chem.* **1976**, *80*, 2641.
[35] R. Hengerer, L. Kavan, P. Krtil, M. Grätzel, *J. Electrochem. Soc.* **2000**, *147*, 1467.
[36] L. C. Wang, N. R. de Tacconi, C. R. Chenthamarakshan, K. Rajeshwar, M. Tao, *Thin Solid Films* **2007**, *515*, 3090.
[37] E. Galoppini, J. Rachfoprd, H. H. Chen, G. Saraf, Y. C. Lu, A. Hagfeldt, G. Boschloo, *J. Phys. Chem. B* **2006**, *110*, 16159.
[38] T. P. Chou, Q. Zhang, B. Russo, G. E. Fryxell, G. Cao, *J. Phys. Chem. C.* **2007**, *111*, 6296.
[39] Y. Diamant, S. G. Chen, O. Melamed, A. Zaban, *J. Phys. Chem. B* **2003**, *107*, 1977.
[40] A. Kongkanand, R. M. Dominguez, P. V. Kamat, *Nano Lett.* **2007**, *7*, 676.
[41] M. Law, L. E. Greene, A. Radenovic, T. Kuykendall, J. Liphardt, P. Yang, *J. Phys. Chem. B* **2006**, *110*, 22652.
[42] Y. Diamnat, S. Chappel, S. G. Chen, O. Melamed, A. Zaban, *Coord. Chem. Rev.* **2004**, *248*, 1271.
[43] G. Boschloo, L. Häggman, A. Hagfeldt, *J. Phys. Chem. B* **2006**, *110*, 13144.
[44] A. Zaban, M. Greenshtein, J. Bisquert, *ChemPhysChem* **2003**, *4*, 859.